A Continuous Polydisperse Thermodynamic Algorithm for a Modified Flory–Huggins Model: The (polystyrene + nitroethane) Example

HERMÍNIO C. DE SOUSA,* LUÍS P. N. REBELO

Departamento de Química, Centro de Química Fina e Biotecnologia, Faculdade de Ciências e Tecnologia da UNL, 2825-114 Caparica, Lisboa, Portugal

Received 9 July 1999; revised 17 November 1999; accepted 24 November 1999

ABSTRACT: A modified Flory–Huggins model is presented, considering a concentration- and temperature-dependent interaction parameter, and using the methodology of Continuous Thermodynamics to take into account both polydispersity and its effect on phase equilibrium of polymeric systems. This model describes all commonly found, as well as other unusual polymer + solvent and polymer + polymer, liquid–liquid phase diagrams and is easily extended to take all possible pressure effects into consideration. Modeling and least-squares fit of polystyrene + nitroethane liquid–liquid cloud-point data have produced results in good accord with the experimental ones by using meaningfully physical parameters. These results have been used to discuss polystyrene molecular weight, pressure, and isotopic substitution effects on polystyrene + nitroethane systems. A first-order interpretation of phase equilibrium isotopic substitution effect has also been applied. It combines the simplest form of the Flory–Huggins model with the statistical theory of condensed phase isotope effects. © 2000 John Wiley & Sons, Inc. J Polym Sci B: Polym Phys 38: 632–651, 2000

Keywords: polymer solutions; liquid–liquid demixing; isotope and pressure effects; generalized Flory–Huggins model; continuous thermodynamics; polydispersity

INTRODUCTION

Modeling of many polymer manufacturing processes requires knowledge of phase equilibria in multicomponent systems containing polymers and solvents. Polymeric systems often exhibit liquid–liquid phase separation, which depends significantly on temperature, composition, pressure, polymer molecular weight, and molecular weight distribution. Although polymer solution liquid–liquid equilibrium (LLE) is of importance for practical applications, it has not until recently received as much attention as vapour–liquid equilibrium (VLE) studies. LLE in polymeric systems is expected to be harder to represent and study than that of solutions of low-molecular-weight species, since systems involving polymers frequently exhibit more types of unusual behavior in solution and polydispersity as well.[1–6]

LLE in polymeric systems is usually represented by an isobaric temperature versus composition phase diagram, where composition is normally presented in terms of weight fraction, volume fraction, or segment fraction. In Figure 1, we represent eight typical shapes of LLE phase diagrams commonly found for polymeric systems, although they can be grouped in a lower number of distinct classes. Demixing in polymer solutions and blends may occur both upon cooling at low

Correspondence to: L. P. N. Rebelo (E-mail: luis.rebelo@dq.fct.unl.pt)

* *Present address:* Departamento de Engenharia Química, Universidade de Coimbra, Polo II, Pinhal de Marrocos, 3020 Coimbra, Portugal

Journal of Polymer Science: Part B: Polymer Physics, Vol. 38, 632–651 (2000)

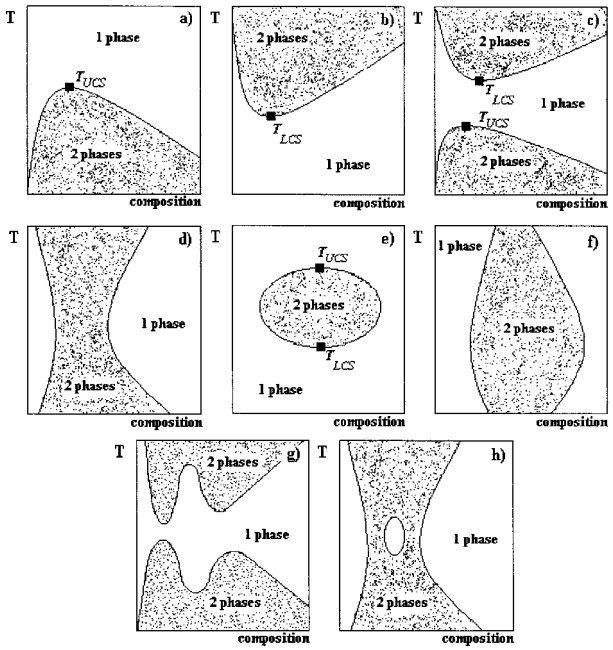

Figure 1. Types of LLE phase diagrams found for polymeric systems (polymer + solvent and polymer + polymer). (a) UCST type; (b) LCST type; (c) combined UCST + LCST type; (d) "hourglass" type; (e) "closed-loop" type; (f) distorted "closed-loop" type; (g) bimodal combined UCST + LCST type; (h) "hourglass" with a miscibility gap type. T_{UCS} and T_{LCS} are the upper and the lower critical solution temperatures, respectively.

temperatures (presenting an upper critical solution temperature, UCST) [Fig. 1(a)], or upon heating at high temperatures (presenting a lower critical solution temperature, LCST) [Fig. 1(b)]. Most systems exhibit both UCST and LCST phase separation [Fig. 1(c)]. In polymeric systems, this phase diagram is the rule rather than the exception, and the individual appearance of only UCST or only LCST can be attributed either to experimental limitations or to difficulties in reaching metastable regions. In some special cases (nontheta, poor solvents), LCST and UCST can merge after reaching one point (called hypercritical temperature point) by searching for a convenient set of values of pressure, polymer molecular weight, and isotope substitution on the solvent or on the polymer [Fig. 1(d)]. These phase diagrams are usually referred as the "hourglass" type. Frequently, LCST lies above UCST, however. When specific interactions are present (e.g., hydrogen bonding in aqueous polymer solutions), a "closed-loop" phase diagram appears with the UCST lying above LCST [Fig. 1(e)]. Other types of unusual LLE phase diagrams can also be found in polymeric systems like those exhibiting a distorted "closed-loop" [Fig. 1(f)], bimodality [Fig. 1(g)], and miscibility "islands" [Fig. 1(h)]. Experimental examples and theoretical predictions of the abovementioned types have been compiled and studied[1,4,7–12] in several works.

Certain variables such as pressure, polymer molecular weight, and isotope substitution, in addition to other factors associated with polymer polymolecularity (polydispersity, tacticity, branching, crosslinking, chain ending groups, etc.) may have a great effect (sometimes drastic) on polymer + solvent and polymer + polymer miscibility. Because of this high complexity, phase equilibrium behavior of polymeric systems and, particularly that of polymer + solvent systems, has drawn considerable attention from polymer physical chemists and engineers and extensive work has been done concerning both theoretical and practical aspects during the last decades.

This work is part of a broad research program, which includes the experimental determination and the prediction and theoretical interpretation of liquid–liquid phase diagrams of polymer + solvent systems, where the effects of MW, pressure, polydispersity, and isotope substitution are considered. Very recently, we reported[13] experimental liquid–liquid cloud-point and spinodal data for polystyrene (PS) + nitroethane systems as a function of pressure, PS molecular weight and isotope substitution on PS and/or nitroethane.

In this article, we present a semiempirical phase equilibrium algorithm based on a modified Flory–Huggins model with a concentration- and temperature-dependent interaction parameter. It takes account of polymer polydispersity by using the methodology of Continuous Thermodynamics. This model, which is based on the work of Qian and collaborators,[6,14] adds the methodology of Ratzsch and co-workers.[15] The algorithm developed herein permits us to portray commonly found polymer + solvent phase diagrams and to understand the effect of polydispersity on these diagrams. Using this algorithm and some robust fitting computer routines we have successfully modeled experimental data obtained for PS + nitroethane[13] and, therefore, have obtained interaction parameters directly from experimental LLE data.

The broader capabilities of the model have already been demonstrated in a previous work,[4] although the details of it were not presented there. This is done in the current work.

MODELS FOR LLE IN POLYMER SOLUTIONS

The common problem to be solved when tackling LLE studies consists in determining at which set of conditions phase separation occurs. From a theoretical point of view, this can be accomplished by searching the set of conditions where the second derivative of the Gibbs free energy of mixing in respect to composition is no longer positive (borderline between metastability and material instability). For this purpose, it is necessary to achieve either an accurate expression for the excess Gibbs free energy or an equation of state (EoS). An optimum model or method should be capable of predicting and representing both VLE and LLE over a wide range of concentrations, pressures, and temperatures, and it should take polymer molecular weight and molecular weight distribution into account. It should also have a reasonably small number of parameters, which should have physical meaning.

During the past decades, since the pioneering work of Chang,[16] Flory,[17] Huggins,[18] and Guggenheim[19] in the 1940s and 1950s, many thermodynamic theories and models of phase separation in polymeric systems (including solutions, blends, and melts) have been proposed and developed. Because of the different approaches and underlying theoretical backgrounds these theories and models have been classified in several distinct ways.

Following the classification proposed by Saraiva,[9,20] two main different approaches can be considered: (1) qualitative and/or semiquantitative descriptions of LLE in terms of polymer solubility, where the main purpose is to predict whether or not a polymer is soluble in a certain solvent (or mixture of solvents) at certain conditions; (2) quantitative and qualitative descriptions of LLE, attempting to establish dependencies of LLE with temperature, composition, and pressure.

The first group of theories and models includes Hildebrand's original solubility parameter theory and its extension to hydrogen bonding and polar compounds,[21] the Shultz–Flory representation[22] and other empirical predictive methods and "rules-of-thumb."[23]

The second category is much more extensive. It comprises the classical Flory–Huggins model[17,18] as well as its extensions and modifications;[1,6,8,14,24] all the lattice-fluid (LF) based models and theories (including the hole theory,[25] the mean-field-lattice-gas models,[26] the well-known Sanchez–Lacombe lattice-fluid EoS and derived models,[27] and the cell theory[28]); all the perturbation theory based models (including the perturbed-hard-chain theory, PHCT, and the perturbed-soft-chain theory,[29] PSCT, the statistical-associating-fluid theory,[30] SAFT, the perturbed-hard-sphere chain,[31] PHSC, and the chain-of-rotators theory,[32] COR); the corresponding states EoS,[33] UNIFAC models,[34] and UNIQUAC models.[35] Recent models using a modified van der Waals EoS to polymer systems[9,36] occur here as well.

Deveke,[8] Saraiva,[9] and Vimalchand and Donohue[37] have reviewed the main characteristics and applicability of some of these theories and models. These models have mostly been applied for the correlation and understanding of polymer solutions and blends. In many cases, the models are rather complex and their performance and predictive capabilities are not yet extensively investigated and exploited. So far, none of the available models are entirely engineering oriented, that is, both simple to apply and reasonably accurate and, therefore, have not been broadly used in polymer technology research and development. An important question remains: is there any good theory, or treatment, of solutions that can be both comprehensive in scope and accurate in its representation of equilibrium properties? Instead of seeking a theory, which is accurate in detail as well as comprehensive in scope, it may be more fruitful to adopt a simpler treatment of reasonable generality at the sacrifice of representation of individual cases.[38] We decided to follow this last route and have adopted a semiempirical model based on the classical Flory–Huggins model but with a concentration- and temperature- (and pressure-) dependent interaction parameter.

The Classical Flory–Huggins Model: Background and Modifications

The well-known Flory–Huggins (FH) expression[17,18] for the Gibbs energy of mixing per volume unit for a monodisperse polymer, B, in one single solvent, A, is given by:

$$\frac{\Delta G_m}{RT} = \frac{\phi_A}{V_A} \ln \phi_A + \frac{\phi_B}{V_B} \ln \phi_B + \chi \phi_A \phi_B \qquad (1)$$

where V_i is the molar volume of component i, ϕ_i is the volume fraction of component i, R is the gas constant, T is the absolute temperature, and χ

is the Flory–Huggins parameter, $\chi = \chi_{FH}/RT$. In the classical lattice FH model, χ_{FH} is concentration- and temperature-independent. This model contains many of the fundamentals of polymer solution phase equilibria but is not capable of describing, even qualitatively, the different types of phase diagrams found in polymer + solvent systems. One of these deficiencies is the inability to describe and explain the appearance of LCST curves. This fact is due to the incompressible nature of the model. Generally, with the exception of water, the free-volume percentage (or compressibility) of a low-molecular-weight compound is greater than the free-volume percentage of a macromolecule. In the case of polymer solutions, the difference in degree of thermal expansion between polymer and solvent increases as temperature increases, attaining very high values as the temperature approaches the gas–liquid critical temperature of solvent. Phase separation is then induced by the expansion of the solvent that takes place with the consequent volume fluctuations. At these conditions, the extremely negative entropy of mixture (unfavourable effect) will overcome the negative value (favourable effect) of the enthalpy of mixture. Excess volumes of mixture are expected to be negative[39] providing dT/dp of the LCST transition is positive.[40]

As mentioned above, because of its simplicity this model displays several failures. It assumes that the FH interaction parameter is independent of concentration, temperature and pressure. However, one knows from experiments that this is not true and it may depend, sometimes in a complex way, on these variables. To eliminate these limitations, several authors suggested the insertion, in a semiempirical way, of the concentration- and temperature-dependency in the FH interaction parameter. These empirically modified FH models possess some theoretical background and their main advantage consists in their simplicity and ability to reproduce VLE and LLE experimental data (even for complex systems).[41]

Let us then write a more general expression for the Gibbs energy of mixing, per volume unit, for a monodisperse polymer, B, in one single solvent, A:

$$\frac{\Delta G_m}{RT} = \frac{\phi_A}{V_A} \ln \phi_A + \frac{\phi_B}{V_B} \ln \phi_B + g(\phi_B, T)\phi_A\phi_B \quad (2)$$

where the FH interaction parameter is now replaced by a function of concentration and temperature, $g(\phi_B, T)$. This dependence can be considered in many different ways.[1,3–5,12,42] Following Orwoll,[43] the relation between the function, $g(\phi_B, T)$ and the FH interaction parameter, $\chi(\phi_B, T)$, is given by:

$$\int_{\phi_B}^{1} \chi(\phi, T)\, d\phi = (1 - \phi_B) g(\phi_B, T) \quad (3)$$

It is easy to show that these two functions, $g(\phi_B, T)$ and $\chi(\phi_B, T)$, only coincide when $g(\phi_B, T)$ is concentration-independent. Note that $g(\phi_B, T)$ is the mean value of $\chi(\phi_B, T)$ in respect to concentration between $\phi = \phi_B$ and $\phi = 1$. Combining eqs 2 and 3:

$$\frac{\Delta G_m}{RT} = \frac{\phi_A}{V_A} \ln \phi_A + \frac{\phi_B}{V_B} \ln \phi_B + \phi_B \int_{\phi_B}^{1} \chi(\phi, T)\, d\phi \quad (4)$$

The expressions for chemical potentials of components A and B can be easily derived:

$$\frac{\Delta \mu_A}{RT} = \ln(1 - \phi_B) + \phi_B\left(1 - \frac{V_A}{V_B}\right) + \chi(\phi_B, T) V_A \phi_B^2 \quad (5)$$

$$\frac{\Delta \mu_B}{RT} = \ln \phi_B + (1 - \phi_B)\left(1 - \frac{V_B}{V_A}\right) - V_B\phi_B(1 - \phi_B)\chi(\phi_B, T) + V_B \int_{\phi_B}^{1} \chi(\phi, T)\, d\phi \quad (6)$$

where Δ refers to the difference between the chemical potential in solution and that of the standard state. Now, according to the approach of Qian and co-workers,[6,14] we can suppose that $\chi(\phi_B, T)$ is a function of a product between a concentration function, $B(\phi_B)$, and a temperature function, $D(T)$:

$$\chi(\phi_B, T) = B(\phi_B) D(T) \quad (7)$$

One of the advantages of this approach is that one can find in the literature experimental interaction parameter data (obtained by other methods) and represent them as a function of temperature and concentration.[43,44] The more realistic and applied forms for the functions $B(\phi_B)$ and

$D(T)$ are[6,14,42] those where b_i and d_i are adjustable parameters:

$$B(\phi_B) = \sum_{i=0}^{n} b_i \phi_B^i \tag{8}$$

$$D(T) = d_0 + \frac{d_1}{T} + d_2 \ln T \tag{9}$$

Under certain thermodynamic conditions, a homogeneous polymer solution or mixture may separate in two or more phases. The conditions for the equilibrium between two phases (marked as I and II) in a binary monodisperse component system (A and B) are expressed by the well-known identity of the chemical potentials of each species, A and B, between the distinct phases I and II:

$$\Delta\mu_A^I = \Delta\mu_A^{II} \tag{10}$$

$$\Delta\mu_B^I = \Delta\mu_B^{II} \tag{11}$$

The manipulation of equations 5–11 reveals:

$$D(T)_A = \frac{\ln\left(\frac{1-\phi_B^{II}}{1-\phi_B^I}\right) + (\phi_B^{II} - \phi_B^I)\left(1 - \frac{V_A}{V_B}\right)}{V_A[B(\phi_B^I)\phi_B^{I^2} - B(\phi_B^{II})\phi_B^{II^2}]} \tag{12}$$

$$D(T)_B = \frac{\ln\left(\frac{\phi_B^{II}}{\phi_B^I}\right) + (\phi_B^I - \phi_B^{II})\left(1 - \frac{V_B}{V_A}\right)}{V_B\left[B(\phi_B^{II})\phi_B^{II}(1-\phi_B^{II}) - B(\phi_B^I)\phi_B^I(1-\phi_B^I) - \int_{\phi_B^{II}}^{\phi_B^I} B(\phi)\, d\phi\right]} \tag{13}$$

We now proceed to consider the fact that $D(T)_A$ is equal to $D(T)_B$, no matter the range of concentrations considered.[45] Thus, by simultaneously solving eqs 12 and 13 using a Newton–Raphson numerical method we obtain the coexistence curve. For a known volume fraction in phase I, ϕ_B^I, we can calculate the volume fraction in phase II, ϕ_B^{II}, which satisfies the relation of equality between eqs 12 and 13. With this value, it is a straightforward matter to calculate the temperature at which the two phases are in equilibrium.

The metastability limit of a binary mixture is defined by the spinodal curve, and can be thermodynamically defined by the stability criterion as[46]

$$\frac{\partial^2(\Delta G_m/RT)}{\partial\phi_A^2} = \frac{\partial^2(\Delta G_m/RT)}{\partial\phi_B^2} = 0 \tag{14}$$

The use of the stability criterion in eq 4 leads, then, to the spinodal curve equation:

$$\frac{1}{V_A(1-\phi_B)} + \frac{1}{V_B\phi_B} - D(T)[2B(\phi_B) + \phi_B B'(\phi_B)] = 0 \tag{15}$$

where the prime ($'$) denotes the first derivative of $B(\phi_B)$ in order to ϕ_B.

The critical point of the binary mixture is the point at which cloud point and spinodal curves become identical. Thermodynamically it is defined by:

$$\frac{\partial^2(\Delta G_m/RT)}{\partial\phi_B^2} = \frac{\partial^3(\Delta G_m/RT)}{\partial\phi_B^3} = 0 \tag{16}$$

which is the same as saying:

$$\frac{1}{(1-\phi_B)} + \left(\frac{V_A}{V_B} - 1\right) - D(T)V_A\phi_B[2B(\phi_B) + \phi_B B'(\phi_B)] = 0 \tag{17}$$

$$-\frac{1}{(1-\phi_B)^2} + D(T)V_A[2B(\phi_B) + 4\phi_B B'(\phi_B) + \phi_B^2 B''(\phi_B)] = 0 \tag{18}$$

where prime ($'$) and double prime ($''$) denote the first and the second derivatives, respectively, of $B(\phi_B)$ in respect to ϕ_B. Solving simultaneously these two equations allow us to obtain the critical temperature(s), T_c, and the critical volume fraction, ϕ_{Bc}.

This simple approach generates commonly found LLE phase diagrams of monodisperse polymer + solvent and polymer + polymer systems as well as other unusual types of phase diagrams like those with occurrence of multiple critical points, coalescence of cloud-point curves, and the appearance of bimodality in cloud-point and spinodal curves.[4,6,14,47] This can be done by choosing the appropriate magnitudes and signs of the parameters, b_i and d_i. However, when modeling ex-

perimental data, some care has to be taken, especially when extrapolating beyond the experimental fitted range.

A Continuous Polydisperse Thermodynamic Modified Flory–Huggins Model

All the material above described considers the polymer to be monodisperse, therefore truly binary mixtures. However, polymers do not have a well-defined molecular weight but a range (distribution) of molecular weights (polydispersity). Therefore, a solution of one polymer in one single solvent does not behave as a true binary mixture but as a multicomponent system of species chemically similar but differing in the polymerization degree. Usually these systems are described as quasibinary or pseudobinary. Polymer polydispersity might have a large effect in the thermodynamic properties and in LLE of polymer solutions.[1,15,47,48] For example, the binodal curve of a true binary polymer + solvent system splits in three different kinds of curves if the system is considered as polydisperse: a cloud-point curve, a "shadow" curve and an infinite number of coexistence curves.[15] This is illustrated in Figure 2. Starting from the homogeneous region, at a given temperature, T, and composition, ϕ_B^I, upon decreasing temperature until reaching the cloud-point curve, at T_{cp}, the (overall) polymer content of the first droplets of the precipitated phase does not correspond to a point on the cloud-point curve but to a corresponding point on the shadow curve, ϕ_B^{II}. Upon lowering temperature further, the equilibrium phases change their compositions neither according to the cloud-point curve nor to the shadow curve but rather according to the related branches of the coexistence curves. These are divided in two branches and just one of them is continuous: the one passing through the critical point. At this point, the cloud-point curve, the shadow curve and the spinodal curve (not represented on Fig. 2) intersect. Thus, the critical point does not correspond to the maximum of the cloud-point curve (as is the case for strictly binary systems).

This complicated behavior is due to polymer polydispersity. Polymers in coexisting phases also present different mean molecular weights distributions and, therefore, may present distinct molecular weight distributions. The cloud-point curve always refers to both the molecular weight and molecular weight distribution of the initial polymer but this does not occur with the first

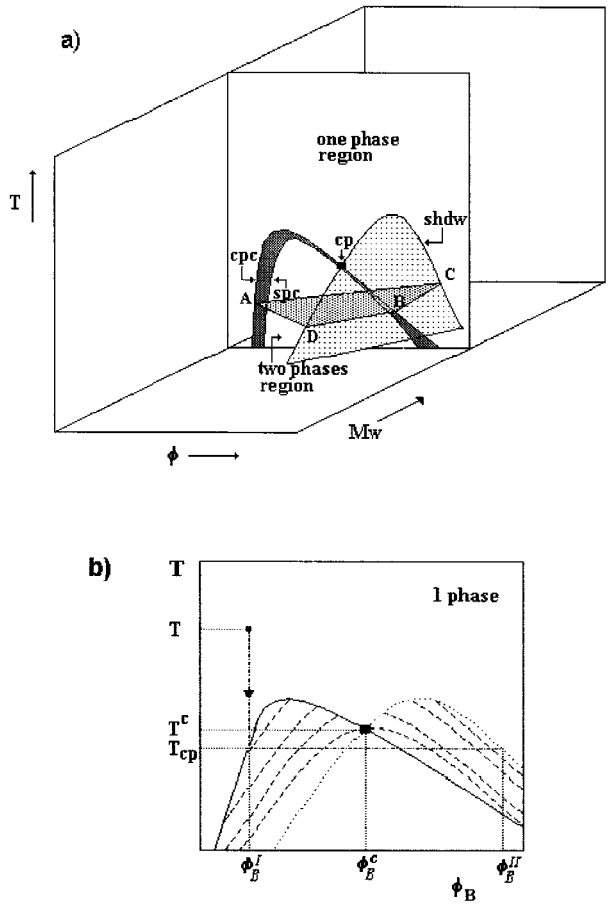

Figure 2. (a) Typical LLE phase diagram in the (T, ϕ, MW) space at constant pressure for a polydisperse polymer + solvent. *Spc* is the spinodal curve. *Cpc* is the cloud-point curve. *Cp* is the critical point. *Shdw* is the shadow curve. *A* is in equilibrium with *C* and and *B* is in equilibrium with *D*. (b) T, ϕ_B projection of a polydisperse system at constant pressure. (—) Cloud-point curve; (· · ·) shadow curve; (- - -) coexistence curves; (■) critical point.

droplets formed on the shadow curve. Such droplets contain polymer with different molecular weight (and molecular weight distribution) from the initial polymer.

Let us consider now that polymer, B, is polydisperse. Equation 4 should be rewritten:

$$\frac{\Delta G_m}{RT} = \frac{\phi_A}{V_A} \ln \phi_A + \sum_{i=1}^{n} \frac{\phi_{Bi}}{V_{Bi}} \ln \phi_{Bi} + \phi_B \int_{\phi_B}^{1} \chi(\phi, T)\, d\phi \quad (19)$$

where V_{bi} and ϕ_{Bi} are, respectively, the molar volume and the volume fraction of component i of polymer B. ϕ_B is the total volume fraction of polymer B. Polydispersity effect does not have a significant effect on the interaction parameter,[49] $\chi(\phi_B, T)$, and thus its effect it is not considered in the last term of eq 19. The equilibrium conditions between two phases, denoted as I and II, are given by:

$$\Delta\mu_A^I = \Delta\mu_A^{II} \tag{20}$$

$$\Delta\mu_{Bi}^I = \Delta\mu_{Bi}^{II}, \quad 1 \le i \le n \quad (n \text{ equations}) \tag{21}$$

and the resolution of the equilibrium criteria becomes impracticable because of the very high number of equations involved, $(n + 1)$.

Therefore, in this work we decided to introduce the methodology of Continuous Thermodynamics into the model described above.[10,47] This method is highly useful in the thermodynamic treatment of polydisperse systems like crude oils and derivatives, vegetable oils and synthetic polymers. In the referred cases, "polydisperse" means that these systems possess a great number of chemically similar species differing just in the molecular weight of the components. Some particular applications have been developed during the last decades but only recently have the fundamentals of Continuous Thermodynamics been well-established[50] and the advantages of the method recognized.[1,51]

Following Ratzsch and co-workers,[15] which developed the application to LLE of polymer + solvent systems, let us rewrite[10,47] eq 19:

$$\frac{\Delta G_m}{RT} = \frac{\psi_A}{r_A}\ln\psi_A + \int \frac{\psi_B W_B(r)}{r}\ln(\psi_B W_B(r))\,dr + \psi_B\int_{\psi_B}^{1}\chi(\psi, T)\,d\psi \tag{22}$$

where ΔG_m is now the Gibbs energy of mixing but per segment unit, ψ_A and ψ_B are the segment fractions of solvent A and polymer B, respectively r_A is the solvent segment number (usually considered as unity, since it is assumed that a solvent molecule has the same size of a polymer monomeric unit) r is the segment number and $W_B(r)$ is the continuous and intensive distribution function of polymer segment number. Once again, the polydispersity effect is not considered in the interaction parameter, $\chi(\phi_B, T)$, and is thus not a function of the segment number r.

The expressions for chemical potentials of components A and B can again be derived, resulting in:

$$\frac{\Delta\mu_A}{RT} = \ln(1 - \psi_B) + \left(1 - \frac{r_A}{\bar{r}}\right) + r_A\psi_B^2\chi(\psi_B, T) \tag{23}$$

$$\frac{\Delta\mu_B(r)}{RT} = \ln[\psi_B W_B(r)] + \left(1 - \frac{r}{\bar{r}}\right) - r\psi_B(1 - \psi_B)\chi(\psi_B, T) + r\int_{\psi_B}^{1}\chi(\psi, T)\,d\psi \tag{24}$$

where $\bar{r}$ is the number-average segment number for the considered phase (I or II), defined as:[15]

$$\frac{1}{\bar{r}} = \frac{\psi_A}{r_A} + \frac{\psi_B}{\bar{r}_B} \tag{25}$$

$$\frac{1}{\bar{r}_B} = \int \frac{W_B(r)}{r}\,dr \tag{26}$$

Here, $\bar{r}_B$ is the number-average segment number of polymer, B, and for the considered phase. The equilibrium conditions between two phases, denoted as I and II, will be given by:

$$\Delta\mu_A^I = \Delta\mu_A^{II} \tag{27}$$

$$\Delta\mu_B^I(r) = \Delta\mu_B^{II}(r) \tag{28}$$

These conditions lead to the new equations:

$$D(T) = \frac{\ln\left(\frac{1 - \psi_B^{II}}{1 - \psi_B^I}\right) + \psi_B^{II}\left(1 - \frac{r_A}{\bar{r}_B^{II}}\right) - \psi_B^I\left(1 - \frac{r_A}{\bar{r}_B^I}\right)}{r_A[B(\psi_B^I)\psi_B^{I^2} - B(\psi_B^{II})\psi_B^{II^2}]} \tag{29}$$

$$D(T) = \frac{\ln\left(\frac{\psi_B^{II}W_B^{II}(r)}{\psi_B^I W_B^I(r)}\right) + r\left[\frac{\psi_B^{II} - \psi_B^I}{r_A} + \frac{\psi_B^I}{\bar{r}_B^I} - \frac{\psi_B^{II}}{\bar{r}_B^{II}}\right]}{r\left[B(\psi_B^{II})\psi_B^{II}(1 - \psi_B^{II}) - B(\psi_B^I)\psi_B^I(1 - \psi_B^I) - \int_{\psi_B^{II}}^{\psi_B^I} B(\psi)\,d\psi\right]} \tag{30}$$

If one assumes the distribution function, $W_B(r)$, to be of the Schulz–Flory type, for each phase, one has:

$$W_B(r) = \frac{k^{k+1}}{\bar{r}_B \Gamma(k+1)} \left(\frac{r}{\bar{r}_B}\right)^k \exp\left(-k\,\frac{r}{\bar{r}_B}\right) \quad (31)$$

where Γ is the Gamma Function (defined in its usual mathematical terms). k is defined by:

$$k = \frac{1}{\rho - 1} \quad (32)$$

where ρ is the polymer polydispersity index, which, in turn, is defined by:

$$\frac{1}{\rho} = \frac{\bar{r}_B}{\bar{r}_{Bw}} = 2 - \frac{\bar{r}_{Bz}}{\bar{r}_{Bw}} \quad (33)$$

where $\bar{r}_{Bw}$ and $\bar{r}_{Bz}$, are, respectively, the weight-average segment number and the z-average segment number for polymer B and for the considered phase. On the other hand:

$$\bar{r}_B = \frac{M_n}{M_s}; \quad \bar{r}_{Bw} = \frac{M_w}{M_s} \quad (34)$$

where M_n is the polymer number-average molecular weight, M_w is the polymer weight-average molecular weight, and M_s is the molecular weight of one monomer unit.

For this distribution function, and under certain restritions,[15] it is possible to obtain the symmetry relation:

$$\frac{\psi_B^{II}}{(\bar{r}_B^{II})^{k+1}} = \frac{\psi_B^{I}}{(\bar{r}_B^{I})^{k+1}} \quad (35)$$

Application of eqs 31–35, permits us to solve eq 29 and 30, and therefore obtain the cloud-point and shadow curves.

Other types of polymer distribution functions (different from the Schultz–Flory distribution function) are possible but it could not be possible to do certain simple analytical and mathematical procedures conducing to a symmetry relation like the one expressed by eq 35. This relation greatly simplifies the phase equilibrium algorithm.

In a manner similar to the above-described monodisperse case, one can obtain the spinodal curve equation:

$$\frac{1}{r_A(1-\psi_B)} + \frac{1}{\bar{r}_{Bw}\psi_B} - D(T)[2B(\psi_B) + \psi_B B'(\psi_B)] = 0 \quad (36)$$

Eq 36, together with eq 37,

$$-\frac{1}{r_A(1-\psi_B)^2} + \frac{\bar{r}_{Bz}}{\bar{r}_{Bw}^2\psi_B^2} + D(T)[3B'(\psi_B) + \psi_B B''(\psi_B)] = 0 \quad (37)$$

define the critical point of the mixture.

DISCUSSION

With these two models at hand, one considering the polymer as monodisperse and the other as polydisperse, it is possible to study the effect of polydispersity on LLE phase diagrams. Figure 3(a) illustrates this effect for a UCST type of phase diagram. Polymer polydispersity decreases the miscibility of the system, increasing the temperature of the cloud-point curve. Shadow and spinodal curves are also represented. As mentioned above, the critical point does not correspond to the cloud-point maximum (in the polydisperse case). In Figure 3(b), only cloud-point curves are represented for several distinct values of polydispersity index, ρ. As expected, an increase in polydispersity corresponds to a miscibility decrease. It is not presented here, but this polydispersity effect is larger for greater polymer molecular weights. The number-average molecular weight and all parameters used are the same in all cases, monodisperse and polydisperse. The monodisperse model presented above was slightly modified in order to also use polymer segment fractions. In Figure 4, the polydispersity effect on commonly found phase diagrams for polymer + solvent systems is represented. In some cases, polydispersity has a drastic effect on LLE and miscibility decrease is a commonly found characteristic in all cases presented.

In Figure 5 we represent the number-average segment number of the precipitated phase (phase II), $\bar{r}_B^{II}$, as a function of the polymer segment fraction of the shadow curve, sPS, for different polydispersity indexes, and for the examples presented in Figure 4. The polymer precipitated in phase II does not have the same number-average molecular weight (and consequently the same number-average segment number) of the polymer

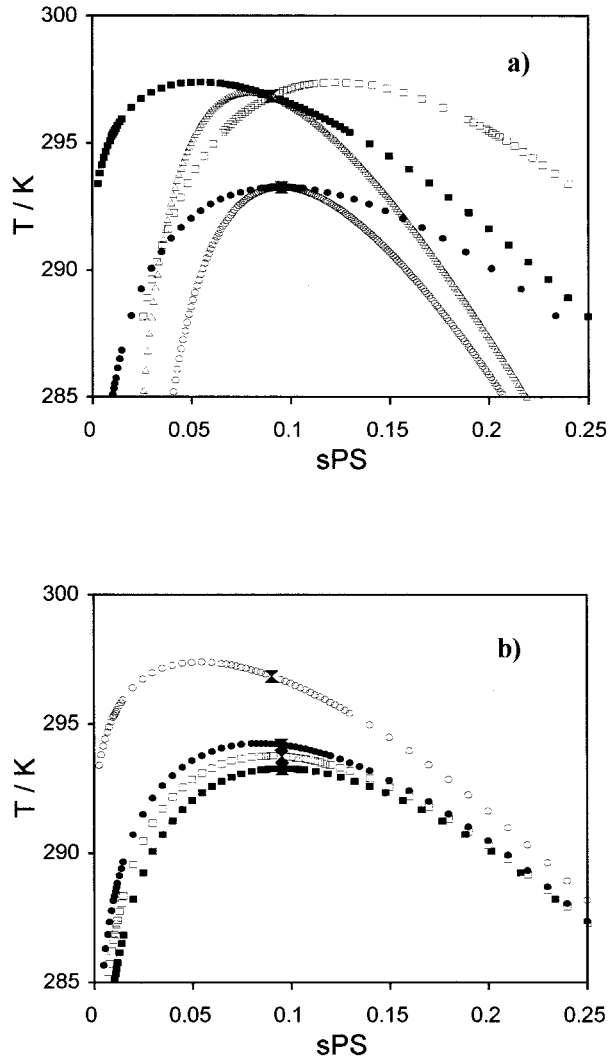

Figure 3. Polydispersity effects on UCST liquid–liquid phase diagrams. (a) Typical polydispersity effect. (●) Cloud-point curve (monodisperse); (○) spinodal curve (monodisperse); (■) cloud-point curve (polydisperse, $\rho = 1.50$); (□) shadow curve (polydisperse, $\rho = 1.50$); (△) spinodal curve (polydisperse, $\rho = 1.50$); (⧗) critical point (monodisperse and polydisperse). (b) Polydispersity effect on cloud-point curves. (■) Cloud-point curve (monodisperse); (□) cloud-point curve (polydisperse, $\rho = 1.05$); (●) cloud-point curve (polydisperse, $\rho = 1.10$); (○) cloud-point curve (polydisperse, $\rho = 1.50$); (⧗) critical point (monodisperse and polydisperse). Used parameters: $b_0 = 1.0$, $b_1 = 0.2$, $b_2 = 0.0$; $d_0 = -0.6$, $d_1 = 345.5$, $d_2 = 0.0$; $M_n = 13{,}000$; $M_s = 104$; $r_A = 1$.

in the initial phase (phase I), except at the critical point. These differences between the number-average segment numbers of phases I and II increase with increasing polydispersity. The possibility of polymer fractionation by equilibrium and phase separation has been known for a long time. One concludes that this model permits us to understand and quantify polymer fractionation due to phase precipitation.

The Polystyrene + Nitroethane Example

Detailed experimental cloud-point and spinodal data for polystyrene + nitroethane systems have been reported in a previous work.[13] With the models described above (monodisperse and polydisperse), we can obtain the concentration- and temperature-dependent interaction parameters of the referred systems. In addition, their shifts due to variation of pressure, MW, and isotope content can be revealed by an appropriate least-squares fit to experimental cloud-point data, adjusting the b_i and d_i parameters. The functional form of the interaction parameter is given by:

$$\chi(\psi_B, T) = B(\psi_B)D(T) = (b_0 + b_1\psi_B + b_2\psi_B^2 + b_3\psi_B^3 + b_4\psi_B^4)\left(d_0 + \frac{d_1}{T} + d_2\ln(T)\right) \quad (38)$$

In Tables I and II, we report these fitted parameters for eight polystyrene + nitroethane systems experimentally studied, at two nominally different pressures, 0.0 and 4.0 MPa, and for the monodisperse and polydisperse cases, respectively. With these adjusted parameters we have calculated spinodal curves, critical temperatures, and critical segment fractions. The latter two quantities are also reported in Tables I and II. For all these systems we have considered: $b_0 = 1$; $b_3 = 0$; $b_4 = 0$; $d_2 = 0$

Number-average molecular weight values and polydispersity indexes were supplied by polystyrene manufacturers and have been reported elsewhere.[13] Nominal values of MW for each studied system as well as polydispersity indexes are found in the tables[13]. Experimental PS weight fractions were converted to PS segment fractions.

In Figure 6(a), the Gibbs free energy of mixing per segment unit, ΔG_m, is plotted as a function of polystyrene segment fraction, sPS. We also represent the coexistence equilibrium segment fractions obtained from identical chemical potentials of each component in the two coexisting phases. The figure clearly shows that it is impossible to graphically detect these points in a ΔG_m curve. The apparent linearity observed in Figure 6(a) is a special and typical feature of LLE of polymer solutions. To identify the hidden curvatures of

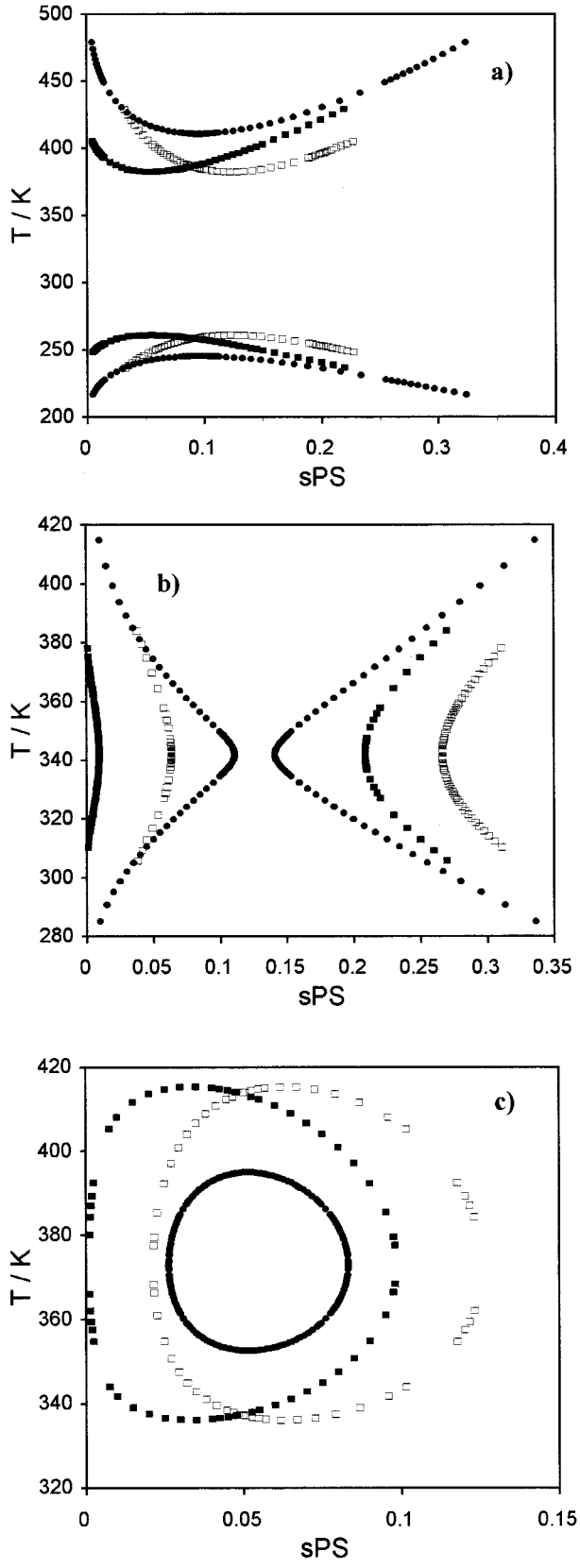

ΔG_m curves, in Figure 6(b) one represents the difference between ΔG_m and the straight line resulting from the connection between the points of stable coexistence equilibrium,[9] $\Delta G_m - F$(sPS), as a function of sPS. This new function permits the clear graphical identification of both the inflection points (spinodal) and minima (binodal).

In Figure 7, modeled LLE phase diagrams are presented together with experimental data for systems I–IV, at 4.0 MPa, considering mono and polydisperse cases. This figure corresponds to the polystyrene molecular weight effect analysis of LLE. Both models conform very well to the experimental cloud-point data. Because of the low polydispersity of our polystyrene samples (we have used polystyrene standards of well-defined molecular weights), modeled cloud-point and shadow curves do not differ much. Fitted b_i and d_i parameters are also not very different in the two approaches (mono and polydisperse). This can be seen in Figure 8 where we can observe the effect of polymer molecular weight on the fitted parameters. Generally speaking, with increasing molecular weight (and the consequent decrease in miscibility, and critical concentration), the b_1 parameter increases, b_2 decreases, d_0 increases initially and then stays approximately constant and d_1 decreases initially and then also keeps roughly constant.

Comments on the Pressure Dependence of Parameters and Their Physical Meaning

It has very recently been shown[40] that the simplest excess Gibbs energy model capable of representing all types of basic LL phase diagrams and all their possible general pressure dependencies is one corresponding to eq 38 in which d_0 is a linear function of pressure, d_1 has a quadratic

Figure 4. Polydispersity effects on other liquid–liquid phase diagrams. Comparison between monodisperse and polydisperse systems. (●) Cloud-point curve (monodisperse); (■) cloud-point curve (polydisperse, ρ = 1.50); (□) shadow curve (polydisperse, ρ = 1.50). (a) Combined UCST + LCST type. Used parameters: b_0 = 1.0, b_1 = 0.2, b_2 = 0.0; d_o = −6.8829, d_1 = 345.5, d_2 = 1.1; M_n = 13,000; M_s = 104; r_A = 1. (b) "Hourglass" type. Used parameters: b_0 = 1.0, b_1 = 0.653, b_2= 0.0; d_0 = −6.9933, d_1 = 376.2, d_2= 1.1; M_n = 23500; M_s = 104; r_A = 1. (c) "Closed-Loop" type. Used parameters: b_0 = 1.0, b_1 = 0.65, b_2= 0.0; d_0 = 2.582; d_1= − 111.9, d_2 = −0.3; M_n = 140,000; M_s = 46.94; r_A = 1.

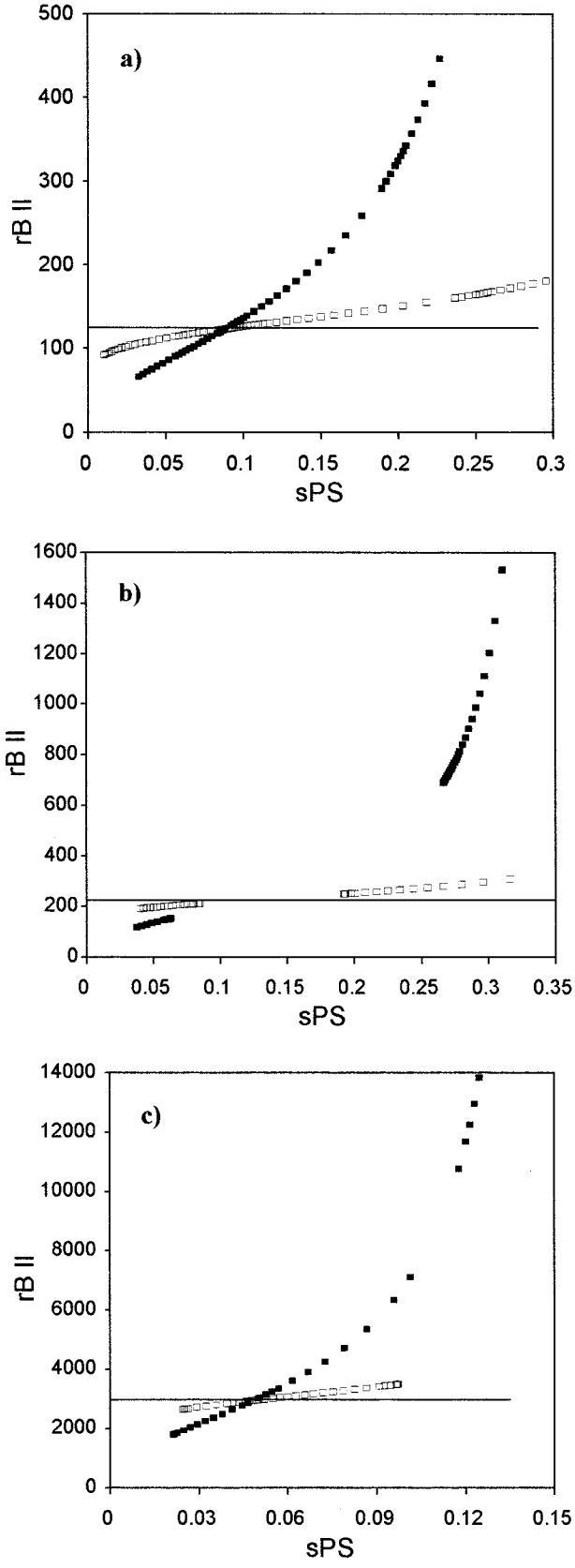

dependence on it, and d_2 is a constant. In other words,

$$\chi(\psi_B, T, p) = B(\psi_B)D(T, p) = B(\psi_B) \times \left(c + b_1 p + \frac{(a_0 + a_1 p + a_2 p^2)}{T} - c_0 \ln(T) \right) / R \quad (39)$$

An expression such as that given by eq 39 can generate all four basic types of (T,p) critical loci including some that have never been experimentally proven.[40] It is a straightforward matter to show that the underlying excess properties such as the excess volume and excess enthalpy are given, respectively, by:

$$v^E(\psi_B, T, p) = B(\psi_B)(a_1 + 2a_2 p + b_1 T) \quad (40)$$

$$h^E(\psi_B, T, p) = B(\psi_B)(a_0 + a_1 p + a_2 p^2 + c_0 T) \quad (41)$$

The excess volume of the solution should thus be linear in pressure and temperature, whereas the excess enthalpy has to have a quadratic dependence on pressure. The ratio between these two excess functions multiplied by the temperature of critical demixing reveals the numerical value for the pressure dependence of the locus of critical temperature. On the other hand, some parameters in equations (38–41) have a direct physical meaning. While d_2 and c_0 define the excess heat capacity, $C_p^E = c_0 B(\Psi_B) = -R\, d_2\, B(\Psi_B)$, b_1 and a_2

Figure 5. Polydispersity effect on the shadow curve number-average segment number (rB II) as a function of the segment fraction of polymer (sPS) in the shadow curve. Comparison between monodisperse and polydisperse systems. (Solid line) Number-average segment number, polymer B, phase I, cloud-point curve, monodisperse; (■) number-average segment number, polymer B, phase II, shadow curve, ρ = 1.50; (□) number-average segment number, polymer B, phase II, shadow curve, ρ = 1.10. (a) Combined UCST + LCST type. Used parameters: b_0 = 1.0, b_1= 0.2, b_2= 0.0; d_0 = −6.8829, d_1 = 345.5, d_2= 1.1; M_n = 13,000; M_s =104; r_A = 1. (b) "Hourglass" type. Used parameters: b_0 = 1.0, b_1 = 0.653, b_2 = 0.0; d_0 = −6.9933, d_1 = 376.2, d_2 = 1.1; M_n = 23,500; M_s = 104; r_A = 1. (c) "Closed-loop" type. Used parameters: b_0 = 1.0, b_1 = 0.65, b_2 = 0.0; d_0 = 2.582, d_1 = −111.9, d_2 = −0.3; M_n = 140,000; M_s = 46.94; r_A = 1.

Table I. Modeling Results for Atactic Polystyrene + Nitroethane Systems: Monodisperse Case[a]

4.0 MPa							
System[b]	b_0	b_1	b_2	d_0	d_1	ψ_{Bc}	T_c (K)
I	1.0000	0.11585	1.25423	0.35535	59.35046	0.165	279.379
II	1.0000	0.33425	1.09351	0.44152	27.26491	0.159	296.699
III	1.0000	0.49725	0.85068	0.42142	29.41000	0.102	316.207
IV	1.0000	0.51290	0.89042	0.43094	25.86470	0.099	322.099
V	1.0000	0.48376	0.94567	0.45335	20.71253	0.143	339.501
VI	1.0000	0.52850	0.77768	0.22780	82.10817	0.120	287.454
VII	1.0000	0.49071	0.89716	0.43463	24.99186	0.125	311.014
VIII	1.0000	0.30899	1.06937	0.13776	107.99653	0.146	269.219
0.0 MPa							
System[b]	b_0	b_1	b_2	d_0	d_1	ψ_{Bc}	T_c (K)
I	1.0000	0.12416	1.24015	0.44427	35.09139	0.166	279.808
II	1.0000	0.33324	1.09543	0.44381	26.66198	0.159	297.322
III	1.0000	0.50336	0.83392	0.42423	28.53345	0.103	317.315
IV	1.0000	0.51571	0.87922	0.43216	25.55090	0.098	323.458
V	1.0000	0.48640	0.93901	0.45041	21.76868	0.142	341.108
VI	1.0000	0.53026	0.77546	0.22518	83.03379	0.121	288.167
VII	1.0000	0.49065	0.89798	0.43306	25.55727	0.126	311.988
VIII	1.0000	0.30898	1.06941	0.13855	107.92576	0.146	269.570

[a] Parameters of eq 38. The subscript c refers to critical conditions.
[b] System I: a-PS(h_8)-13000 + h_5-nitroethane; System II: a-PS(h_8)-30000 + h_5-nitroethane; System III: a-PS(h_8)-90000 + h_5-nitroethane; System IV: a-PS(h_8)-130000 + h_5-nitroethane; System V: a-PS(h_8)-90000 + d_5-nitroethane; System VI: a-PS(d_8)-90000 + h_5-nitroethane; System VII: a-PS(d_8)-90000 + d_5-nitroethane; System VIII: a-PS(d_8)-26600 + h_5-nitroethane.

are closely related to the excess thermal expansivity and compressibility. Parameters a_1 and a_0 refer, respectively, to the values of the excess volume and excess enthalpy in a hypothetical state at null temperature and pressure.

Because of the small pressure effect on the phase diagrams of (nitroethane + polystyrene), which amounts to about 0.1–0.3 K/MPa at our experimental conditions, it was not possible to accurately define the pressure dependence of parameters d_0 and d_1 (see also Tables I and II) in eq 38. Optimally, one should work near temperature hypercritical points (where dT_c/dp tends to infinity) or substantially augment the range of studied pressures.

Isotope Effects on the Polystyrene + Nitroethane System

In Figure 9, we represent experimental and modeled LLE phase diagrams for some polystyrene + nitroethane systems, at 4.0 MPa, (Systems III, V, VI, and VII) corresponding to systems containing samples with similar polystyrene number-average molecular weight ($M_n \sim 90{,}000$) but with isotope substitution in polystyrene and/or nitroethane. Monodisperse and polydisperse case fits are presented. Isotope substitution on polystyrene (system VI) increases miscibility, whereas isotope substitution on nitroethane (system V) decreases it. Simultaneous deuteration on polystyrene and nitroethane (system VII) does not change remarkably phase equilibrium when compared with the case where both species are protonated (system III). For all these systems, the parameters, b_1 and b_2, do not change markedly with isotope substitution nor do parameters d_0 and d_1 vary a lot, except for system VI. These observations are valid for both the monodisperse and polydisperse approaches (see Tables I and II).

Van Hook and collaborators[1,2,52] have published cloud-point and spinodal data on systems containing polystyrene (perprotonated and perdeuterated) in several solvents (acetone, methylcyclopentane, and propionitrile), also protonated and deuterated. They developed a first-order in-

Table II. Modeling Results for Atactic Polystyrene + Nitroethane Systems: Polydisperse Case[a]

4.0 MPa							
System[b]	b_0	b_1	b_2	d_0	d_1	ψ_{Bc}	T_c (K)
I	1.0000	0.19170	1.13386	0.27015	81.27313	0.180	279.521
II	1.0000	0.35613	1.05616	0.41632	34.22106	0.170	296.774
III	1.0000	0.50706	0.81829	0.40189	35.40242	0.102	316.254
IV	1.0000	0.51083	0.89948	0.43667	24.01365	0.099	322.147
V	1.0000	0.50378	0.90102	0.38578	43.24158	0.148	339.585
VI	1.0000	0.53534	0.75756	0.19993	90.00599	0.119	287.460
VII	1.0000	0.49883	0.87587	0.41964	29.49931	0.126	310.999
VIII	1.0000	0.30315	1.08290	0.17679	97.49265	0.145	269.209
0.0 MPa							
System[b]	b_0	b_1	b_2	d_0	d_1	ψ_{Bc}	T_c (K)
I	1.0000	0.19084	1.13550	0.27256	80.71305	0.180	279.857
II	1.0000	0.35422	1.05972	0.42012	33.20122	0.169	297.400
III	1.0000	0.51399	0.79932	0.39372	38.01322	0.103	317.292
IV	1.0000	0.51328	0.88952	0.43801	23.65634	0.098	323.511
V	1.0000	0.50647	0.89341	0.38881	42.35891	0.145	341.090
VI	1.0000	0.53737	0.75480	0.19679	91.09714	0.120	288.173
VII	1.0000	0.49897	0.87631	0.41755	30.23909	0.126	311.978
VIII	1.0000	0.30309	1.08304	0.17782	97.34170	0.145	269.554

[a] Parameters of eq 38. The subscript c refers to critical conditions.
[b] System I: a-PS(h_8)-13000 + h_5-nitroethane; System II: a-PS(h_8)-30000 + h_5-nitroethane; System III: a-PS(h_8)-90000 + h_5-nitroethane; System IV: a-PS(h_8)-130000 + h_5-nitroethane; System V: a-PS(h_8)-90000 + d_5-nitroethane; System VI: a-PS(d_8)-90000 + h_5-nitroethane; System VII: a-PS(d_8)-90000 + d_5-nitroethane; System VIII: a-PS(d_8)-26600 + h_5-nitroethane.

terpretation of phase equilibrium isotope substitution effect, which combines the main features of the Guggenheim's symmetrical mixtures theory[53] and the statistical theory of condensed phase isotope effects.[54] Here, we adopt the simplest form of the classical FH model, that is, considering a monodisperse polymer, B, and that the interaction parameter, χ_{FH}, is concentration- and temperature-independent. This results for the excess Gibbs energy in:

$$\Delta G^{\text{exc}} = \chi_{FH}\psi_B(1 - \psi_B) \tag{42}$$

At critical concentration, demixing occurs whenever

$$\frac{\chi_{FH}}{RT} \geq 2 \tag{43}$$

Therefore,

$$RT_c = \chi_{FH}/2 \tag{44}$$

The expressions for chemical potentials of components A and B will be:

$$\frac{\Delta\mu_A}{RT} = \ln(1 - \psi_B) + \psi_B\left(1 - \frac{r_A}{r_B}\right) + 2r_A\psi_B^2 \tag{45}$$

$$\frac{\Delta\mu_B}{RT} = \ln(\psi_B) + (1 - \psi_B) \times \left(1 - \frac{r_B}{r_A}\right) + 2r_B(1 - \psi_B)^2 \tag{46}$$

The major contribution for the isotope effect[1,54] comes from the zero-point energy term (B term of Bigeleisen's AB equation[54]):

$$\frac{\delta\Delta\mu_0^\infty}{RT} = \frac{A}{T^2} + \frac{B}{T} \tag{47}$$

$$A = \frac{1}{24}\left(\frac{hc}{k}\right)^2 \sum_i [(\bar{v}_i'^2 - \bar{v}_i^2)^\infty - (\bar{v}_i'^2 - \bar{v}_i^2)^0] \tag{48}$$

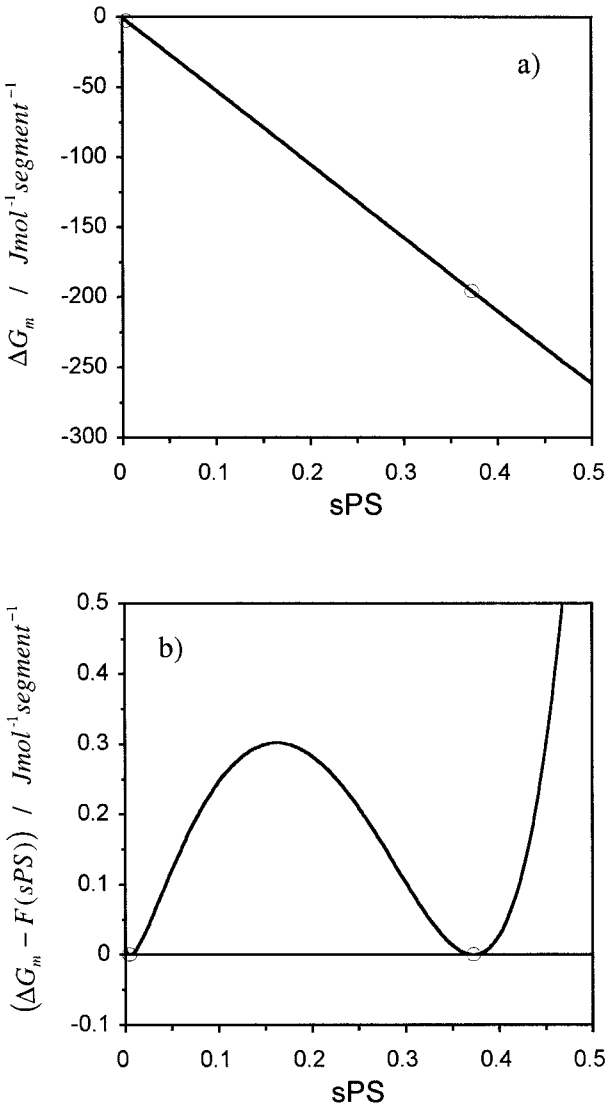

Figure 6. (a) ΔG_m versus sPS curve obtained with the fitted parameters for system III, at 0.0 MPa and 299.26 K (monodisperse model). (—) ΔG_m versus sPS curve; (○) points of stable phase equilibrium. (b) ΔG_m F(sPS) versus sPS curve obtained with the fitted parameters for system III, at 0.0 MPa and 299.26 K (monodisperse model). (—) ΔG_m F(sPS) versus sPS curve; (○) points of stable phase equilibrium.

$$B = \frac{1}{2}\left(\frac{hc}{k}\right) \sum_j [(\bar{\upsilon}_j' - \bar{\upsilon}_j)^{\infty} - (\bar{\upsilon}_j' - \bar{\upsilon}_j)^{0}] \quad (49)$$

where k is the Boltzmann's constant; h, the Planck's constant; c, the velocity of light; and $\bar{\upsilon}$, the wave number. In this case, "′" denotes the lighter isotope. The above equations can be applied when the isotope-sensitive vibrations of the considered molecules fall in two classes: (1) a high-frequency set (indexed over j), which can be treated by the zero-point energy (ZPE) approximation (B term); and (2) a low-frequency set (indexed over i), which includes the external vibrations (hindered translation and rotation), and the internal rotations. This last set can be treated by the high-temperature approximation (A term).

Let us then consider that the major portion of the isotope effect is due to the B term (ZPE), associated with the carbon–hydrogen (C—H) or the carbon–deuterium (C—D) stretching modes, when the molecule is transferred from its pure reference state, o, to infinite dilution in the other component of the mixture, ∞. This way, we can calculate the free transfer energy between these two states.

The transfer from a perprotonated reference state to a perdeuterated solvent state, leads to a transfer energy of:

$$\delta\Delta\mu_{Ac} = (\Delta\mu_{Ac})_{\text{perdeuterated}} - (\Delta\mu_{Ac})_{\text{perprotonated}} \quad (50)$$

On the other hand, the transfer from a perprotonated reference state to a perdeuterated polymer (solute) state, leads to a transfer energy:

$$\delta\Delta\mu_{Bc} = (\Delta\mu_{Bc})_{\text{perdeuterated}} - (\Delta\mu_{Bc})_{\text{perprotonated}} \quad (51)$$

Considering:

$$\delta\Delta\mu_{Ac} = \tfrac{1}{2} n_{Ac} r_A \delta\Delta_0^{\infty}\bar{\upsilon} Nhc \quad (52)$$

$$\delta\Delta\mu_{Bc} = \tfrac{1}{2} n_{Bc} r_B \delta\Delta_0^{\infty}\bar{\upsilon} Nhc \quad (53)$$

it is possible to obtain the vibrational frequency shifts, $\delta\Delta_0^{\infty}\bar{\upsilon}$, associated with the considered isotopic substitution. In this case, n_{ic} is the number of C—H oscillators in a solvent molecule (A) or in a polymer segment (B). r_i is the segment number of solvent (A) or polymer (B) and, N is the Avogadro's number.

Usually, the typical isotope effect for the C—H stretching vibration, in the pure liquid state, is of the order of 800 cm^{-1} and the typical frequency shift for the C—H and C—D stretchings for the liquid–gas phase transition is of the order of 10–14 cm^{-1}. This latter value is comparable to the value of transferring one molecule from its pure reference state to infinite dilution in another component.[54]

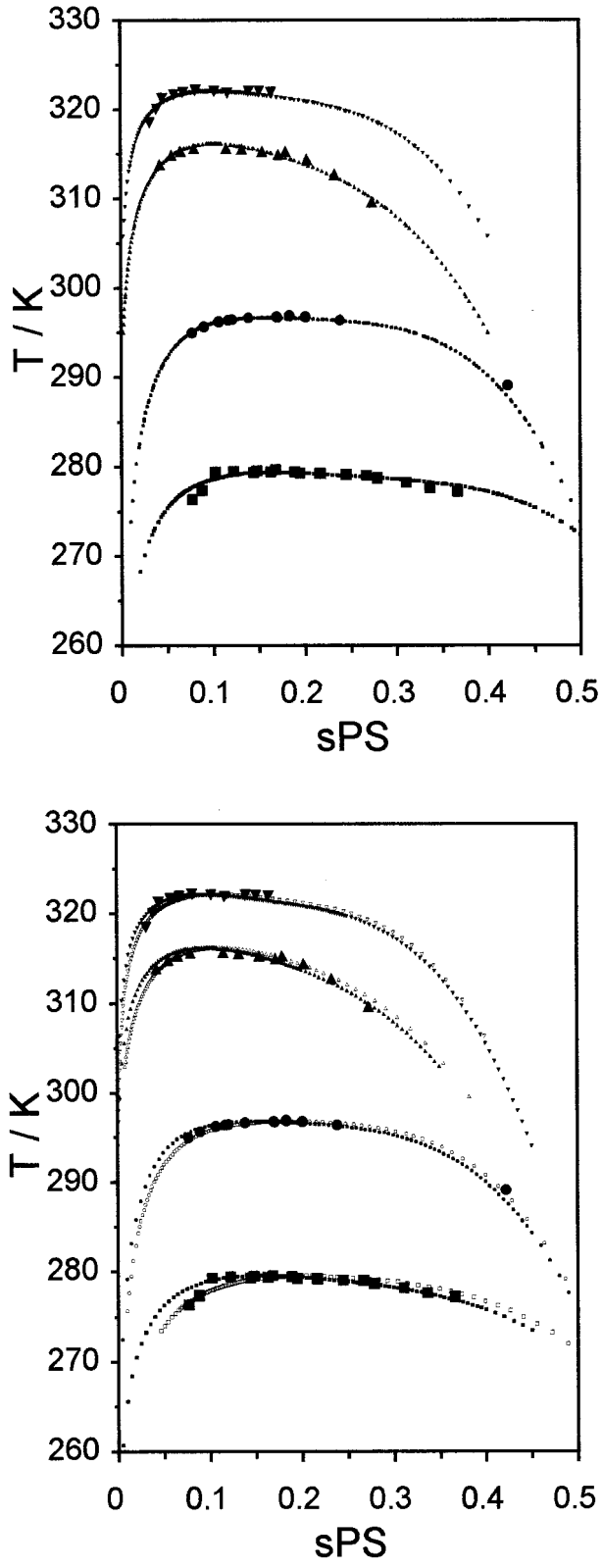

Figure 7. Experimental and modeled LLE phase diagrams for some polystyrene + nitroethane systems (Systems I-IV). Molecular weight effect at 4.0 MPa. Monodisperse (upper) and polydisperse (lower) cases.

Using the above equations and applying them to the systems studied experimentally, reveals that the isotope effect observed for systems III and V [a-PS(h_8)-90000/h_5-nitroethane and a-PS(h_8)-90000/d_5-nitroethane] corresponds to a blue shift of the order of 1.2–1.3 cm^{-1} for each one of the five C—H stretches in the nitroethane molecule. For the polystyrene + acetone system,[1] isotopic substitution on acetone corresponds to a blue shift of the order of 9 cm^{-1} for each one of the six C—H stretches in the acetone molecule. In the case of other systems[1] such as polystyrene + methylcyclopentane and polystyrene + propionitrile this blue shift is of the order of 2 cm^{-1} and 39 cm^{-1}, respectively, for each one of the C—H stretches in the solvent molecule.

In the same way, for the systems III and VI [a-PS(h_8)-90000/h_5-nitroethane and a-PS(d_8)-90000/h_5-nitroethane], the observed isotope effect corresponds to a red shift of the order of 3.2–3.3 cm^{-1} for each one of the eight C—H stretches in a polystyrene segment (considered as a monomer molecule, i.e., styrene.). In the case of the polystyrene + acetone system, isotopic substitution of polystyrene corresponds to a red shift of the order of 7 cm^{-1} for each one of the eight C—H stretches in a polystyrene segment. For polystyrene + methylcyclopentane and polystyrene + propionitrile, this red shift is of the order of 0.5 cm^{-1} and 4 cm^{-1}, respectively, for each one of the eight C—H stretches in a polystyrene segment. For systems II and VIII [a-PS(h_8)-30000/h_5-nitroethane and a-PS(d_8)-26600/h_5-nitroethane], isotopic substitution on polystyrene corresponds to a red shift of the order of 2.8–2.9 cm^{-1} for each one of the eight C—H stretches in a polystyrene segment.

It should be noted that larger shifts are expected to be found in systems experiencing thermodynamic conditions close to hypercritical points, such as those occurring in acetone or pro-

(■) Experimental cloud-point, Syst. I: a-PS(h_8)-13000; (●) experimental cloud-point, Syst. II: a-PS(h_8)-30000; (▲) experimental cloud-point, Syst. III: a-PS(h_8)-90000; (▼) experimental cloud-point, Syst. IV: a-PS(h_8)-130000; (■) cloud-point, modeled, Syst. I: a-PS(h_8)-13000; (●) cloud-point, modeled, Syst. II: a-PS(h_8)-30000; (▲) cloud-point, modeled, Syst. III: a-PS(h_8)-90000; (▼) cloud-point, modeled, Syst. IV: a-PS(h_8)-130000; (□) shadow, modeled, Syst. I: a-PS(h_8)-13000; (○) shadow, modeled, Syst. II: a-PS(h_8)-30000; (△) shadow, modeled, Syst. III: a-PS(h_8)-90000; (▽) shadow, modeled, Syst. IV: a-PS(h_8)-130000.

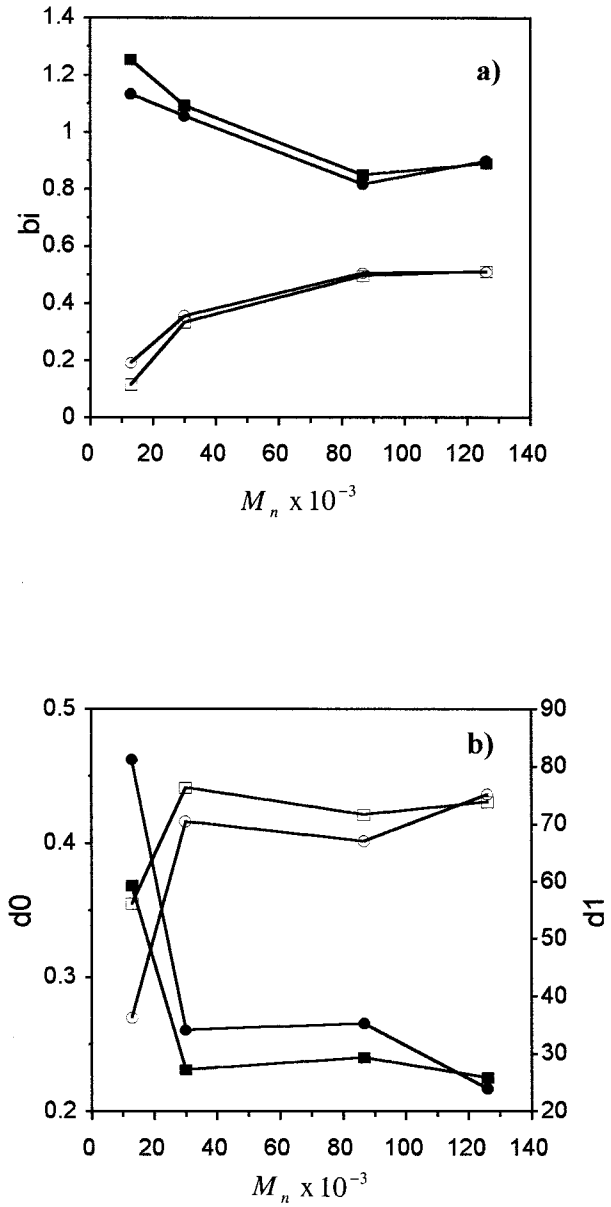

Figure 8. Fitted b_i (case *a*) and d_i (case *b*) parameters for some polystyrene + nitroethane systems (systems I–IV). Molecular weight effect at 4.0 MPa. Monodisperse and polydisperse cases. (—■—) b_2, d_1, monodisperse; (—□—) b_1, d_0, monodisperse; (—●—) b_2, d_1, polydisperse; (—○—) b_1, d_0, polydisperse.

pionitrile. Here, the mixture should experience a large (negative) excess volume.[40] In contrast, phase equilibria of solutions of polystyrene in methylcyclopentane or nitroethane show subtle pressure dependence and, consequently, isotope effects are small.

Some Remarks

The main goal of this article is to present in detail an accurate and efficient methodology capable of dealing with all kinds of behavior presented by liquid–liquid equilibrium in polymeric systems, be they of the monodisperse or polydisperse type. Ways of extending the treatment in order to include pressure and isotope effects are also explained. Since we have clearly demonstrated that the model is completely, generally applicable [see, e.g., Figs. 4 and 5, (a–c)], we decided to focus on the main goal and present just one set of real (closely related) systems. The reason for choosing PS + nitroethane as an example of practical applicability is twofold. First of all, very recently these systems were studied in this laboratory[13] and their raw data published without any theoretical modeling. Furthermore, the set of systems comprised by applying pressure and isotope effects to PS + nitroethane constitutes a nonspecific and possible model case for the most common experimentally found behavior (UCST type). This is well illustrated in Figures 7 and 9, and Tables I and II. Pressure and isotope effects, as well as polymer molecular weight, induce a change in solvent's quality similar to that obtained by its real substitution. In other words, plots like those represented in Figures 7 and 9 could represent the same kind of systems, or not.

Although the detailed description of this methodology has never been previously presented, its application to other specific systems has been successfully checked in preliminary tests. Examples include the very unusual behavior (strongly bimodal) of PS + acetaldehyde,[4] PS + methylcyclopentane[10] or PS + acetone.[47] As new relevant systems become experimentally available, we intend to apply the algorithm herein described in an improved version where pressure is directly taken into account as suggested by eqs 39–41. Luszczyk et al.[1] have reviewed the pertinent literature of modeling pseudobinary mixtures. All those methods referred therein differ in the type of chain-distribution assumed for the polymer, in regard to the model for calculation of multicomponent activity coefficients (and their temperature and pressure dependence), and the numerical strategy applied. The qualities that distinguish this algorithm from others have to do with its very fast numerical convergence, very high precision, and use of a functional temperature[6,14] and pressure (this work, eqs 39–41) form for activity coefficients with obvious meaningful physical mean-

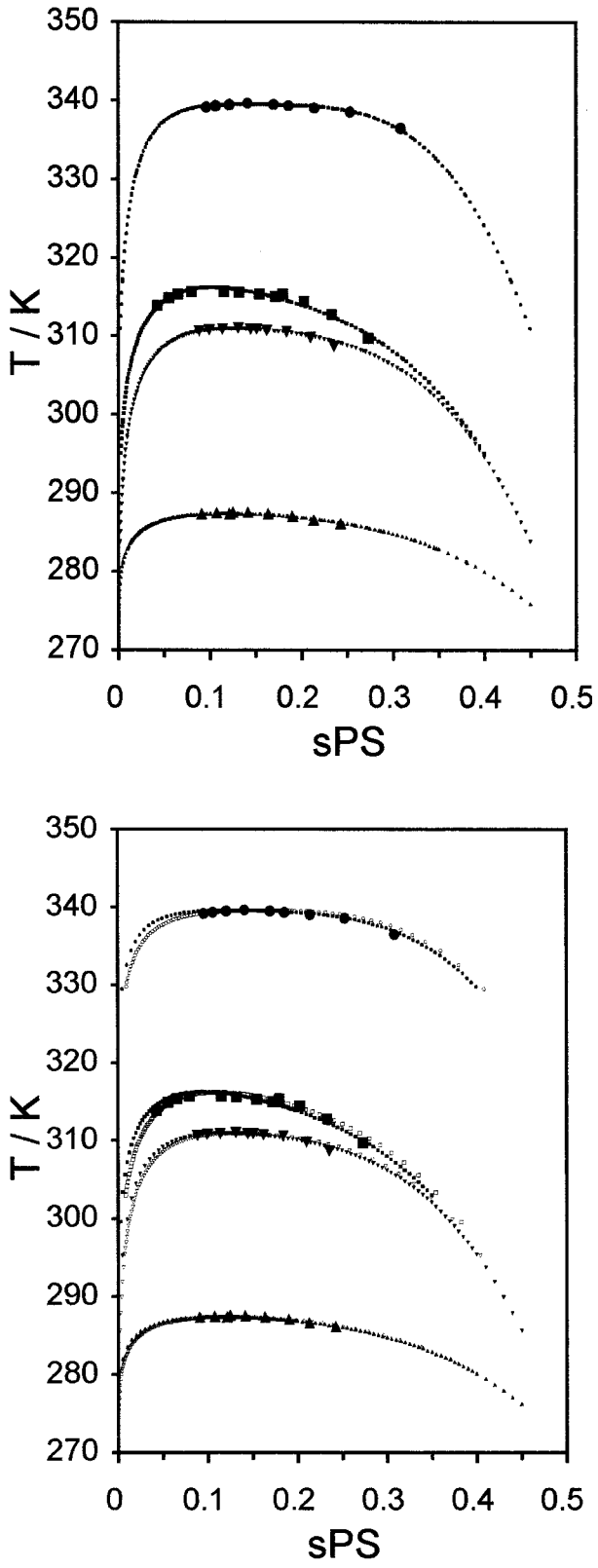

Figure 9. Experimental and modeled LLE phase diagrams for some polystyrene + nitroethane systems (systems III, V, VI and VII: M_n = 90,000). Isotope substitution effect at 4.0 MPa. Monodisperse and polydisperse cases. (■) Experimental cloud-point, Syst. III: a-PS(h_8)/h_5-nitroethane; (●) experimental cloud-point, Syst. V: a-PS(h_8)/d_5-nitroethane; (▲) experimental cloud-point, Syst. VI: a-PS(d_8)/h_5-nitroethane; (▼) experimental cloud-point, Syst. VII: a-PS(d_8)/d_5-nitroethane; (■) cloud-point, modeled, Syst. III: a-PS(h_8)/h_5-nitroethane; (●) cloud-point, modeled, Syst. V: a-PS(h_8)/d_5-nitroethane; (▲) cloud-point, modeled, Syst. VI: a-PS(d_8)/h_5-nitroethane; (▼) cloud-point, modeled, Syst. VII: a-PS(d_8)/d_5-nitroethane; (□) shadow, modeled, Syst. III: a-PS(h_8)/h_5-nitroethane; (○) shadow, modeled, Syst. V: a-PS(h_8)/d_5-nitroethane; (△) shadow, modeled, Syst. VI: a-PS(d_8)/h_5-nitroethane; (▽) shadow, modeled, Syst. VII: a-PS(d_8)/d_5-nitroethane.

ing.[40] The use of a standard Newton–Raphson numerical methodology for solving simultaneously eqs 12 and 13, or 21 and 30 in conjunction with eq 9 through a Borland Pascal program permits us to work at double-precision. Typically, the ultimate increment net is of the order of 10^{-9} in the $D(T)$ functions when searching for solutions in ϕ, and of the same magnitude for T (through eq 9). It is thus possible to use directly the algorithm within a large range of molecular weights and polydispersity indexes without any additional effort.

Finally, we turn now our attention to a brief discussion about comparisons between the monodisperse and polydisperse cases. So far, and throughout the text, comparisons between cases of $\rho = M_w/M_n = 1$ and $\rho > 1$ have been made at fixed M_n. In other words, when comparing the two cases, the value for M_w in the polydisperse solution is greater than that of the monodisperse. As can be seen from analysis of Figures 3 and 4, the effective effect of polydispersity corresponds to one where miscibility decreases. In a UCST type of behavior this translates as follows: as the degree of polydispersity increases, the spinodal moves towards higher temperatures, the critical point to higher temperatures and lower concentrations, as does the cloud-point curve maximum, which is no longer the critical point. Alternatively, one could have compared those cases at fixed M_w. Here, the value of M_n in the polydisperse solution is smaller than that of the monodisperse. In spite of this decrease, miscibility still decreases as previously described. This phenomenon is well illustrated by the analysis of Figure 10. Note that the two spinodal curves are now identical (solutions of eq 36 depend on M_w, not

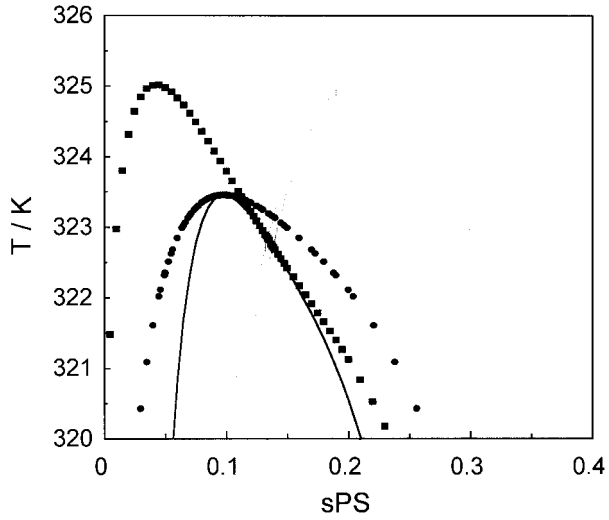

Figure 10. Polydispersity effects on UCST liquid–liquid phase diagrams. Fixing M_w and comparing at distinct M_n. (●) Cloud-point curve (monodisperse); (○) spinodal curve (monodisperse); (■) cloud-point curve (polydisperse, ρ = 1.50); (□) shadow curve (polydisperse, ρ = 1.50); (solid line) Spinodal curve (polydisperse, ρ = 1.50). Used parameters: b_0 = 1.0000, b_1= 0.5157, b_2 = 0.8792; d_0 = −0.4322, d_1= 25.5509, d_2 = 0.0000; M_w = 126,000; M_s = 104; r_A = 1.

M_n). And although the critical point has moved to a slightly lower temperature (and higher concentration), most of the cloud-point curve has moved to higher temperatures and lower concentrations (including its maximum). At this stage, it is still pertinent to ask whether one should compare the two cases at the same M_n or same M_w. It is the authors' opinion that the first option is the most correct. From a theoretical point of view, M_n should always be the reference molecular weight, because it corresponds to a direct counting of the number of segments in a polymer chain (first moment of the molecular weight distribution function). In contrast, M_w, which is the commonly considered molecular weight from an experimental point of view, corresponds to the second moment of the distribution function, and even higher moments could then be considered, such as M_z.

CONCLUSIONS

We have developed an algorithm that permits the modeling of liquid–liquid equilibria in real (polydisperse) polymer solutions. It makes use of a modified semiempirical Flory–Huggins model, which considers a concentration-, temperature-, and the simplest pressure-dependent interaction parameter, and incorporates the methodology of Continuous Thermodynamics. It is capable of describing all the commonly found and other unusual polymer + solvent and polymer + polymer liquid–liquid phase diagrams. Its major improvements and utility are that it can take into account both polymer polydispersity and its effect, sometimes drastic, on these phase diagrams as well as all kinds of expected pressure effects.

With this model, we least-squares fitted polystyrene + nitroethane liquid–liquid experimental data.[13] The fitted curves agree well with the experimental results and permitted us to extract the model adjustable parameters directly from cloud-point data. These results were then used to discuss polystyrene molecular weight and isotope substitution effects on polystyrene + nitroethane systems. A first order interpretation of phase equilibrium isotope substitution effect was applied, which combines the simplest form of the Flory–Huggins model and the statistical theory of condensed phase isotope effects. The observed critical temperature shifts upon isotope substitution are interpreted in terms of the C—H vibrational frequency shifts occurring upon isotope substitution and pure to infinitely diluted reference state.

This work was supported by the Stride Program under Grant #STRDA/C/CTM/626/92. H.C.S. acknowledges JNICT for financial support under Grant # BD/2189/92.

REFERENCES AND NOTES

1. (a) Luszczyk, M.; Rebelo, L. P. N.; Van Hook, W. A. Macromolecules 1995, 28(3), 745–767; (b) Luszczyk, M.; Van Hook, W. A. Macromolecules 1996, 29(20), 6612–6620.
2. Rebelo, L. P. N.; Van Hook, W. A. J Polym Sci Part B: Polym Phys 1993, 31, 895–897.
3. Vanhee, S.; Koningsveld, R.; Berghmans, H.; Solc, K. J Polym Sci Part B: Polym Phys 1994, 32, 2307–2309.
4. Rebelo, L. P.; de Sousa, H. C., Van Hook, W. A. J Polym Sci Part B: Polym Phys 1997, 35, 631–637.
5. Solc, K.; Koningsveld, R. J Phys Chem 1992, 96, 4056–4068.
6. Qian, C.; Mumby, S. J.; Eichinger B. E. Macromolecules 1991, 24, 1655–1661.
7. (a) Sorensen, J. M.; Arlt, W. Liquid–Liquid Equilibrium Data Collection 1. Binary Systems, DECHEMA Chemistry Data Series, Frankfurt, 1979; (b) Danner, R. P.; High, M. S. Handbook of

Polymer Solution Thermodynamics, DIPPR 881 Project, American Institute of Chemical Engineers, New York, 1993.
8. Deveke, D. J. Ph.D. Thesis, Pennsylvania State University, USA, 1993.
9. Saraiva, A. Ph.D. Thesis, Technical University of Denmark, Lingby, Denmark, 1995.
10. de Sousa, H. C. Ph.D. Thesis, New University of Lisbon, Lisbon, Portugal, 1997.
11. Imre, A.; Van Hook, W. A. J Phys Chem Ref Data 1996, 25(2), 637–661.
12. (a) Solc, K.; Stockmayer, W. H.; Lipson, G. E. J.; Koningsveld, R. In Multiphase Macromolecular Systems; Culberston, B. M., Ed.; Plenum Press: New York, 1989; Vol. 6; (b) Solc, K.; Kleintjens, L. A.; Koningsveld, R. Macromolecules 1984, 17, 573.
13. de Sousa, H. C.; Rebelo, L. P. N. J Chem Thermodyn 2000, 32, in press.
14. (a) Qian, C.; Mumby, S. J.; Eichinger, B. E. J Polym Sci Part B: Polym Phys 1991, 29, 635–637; (b) Mumby, S. J.; Qian, C.; Eichinger, B. E. Polymer 1992, 33, 5105; (c) Mumby, S. J.; Sher, P.; Eichinger B. E. Polymer 1993, 34, 2540–2545; (d) Mumby, S. J.; Sher, P. Macromolecules 1994, 27, 689–694.
15. (a) Ratzsch, M. T.; Kehlen, H. Fluid Phase Equilib 1983, 14, 225–234; (b) Ratzsch, M. T.; Kehlen, H.; Bergmann, J. AIChE J 1985, 31(7), 1136–1148 (c) Ratzsch, M. T.; Kehlen, H. Prog Polym Sci 1989, 14, 1–46.
16. Chang, T. S. Proc Cambridge Philos Soc 1939, 35, 265.
17. (a) Flory, P. J.; J Chem Phys 1941, 9, 660–661; (b) Flory, P. J. J Chem Phys 1942, 10, 51–61.
18. (a) Huggins, M. L. J Chem Phys 1941, 9, 440–440; (b) Huggins, M. L. J Phys Chem 1942, 46, 151.
19. Guggenheim, E. A. Mixtures; Clarendon Press: Oxford, UK, 1952.
20. Saraiva, A.; Bogdanic, G.; Fredenslund, Aa. Ind Eng Chem Res 1995, 34, 1835–1841.
21. (a) Hildebrand, J. H. J Chem Phys 1947, 15, 225–228; (b) Hansen, C. M. J Paint Technol 1967, 39, 104–117.
22. Shultz, A. R.; Flory, P. J. J Am Chem Soc 1952, 74, 4760.
23. (a) Fox, T. G. Polymer 1962, 3, 111–128; (b) Van Krevelen, D. W.; Hoftyser, P. J.; J Appl Polym Sci 1967, 11, 2189–2200; (c) Klein, J.; Jeberien, H.-E. Makromol Chem 1980, 181, 1237; (d) Wakker, A.; van Dijk, F.; van Dijk, M. A. Macromolecules 1993, 26, 5088.
24. (a) Koningsveld, R.; Kleintjens, L. A. Macromolecules 1971, 4, 637–641; (b) Solc, K.; Kleintjens, L. A.; Koningsveld, R. Macromolecules 1984, 17, 573–585; (c) Kang, C. H.; Sandler, S. I. Fluid Phase Equilib 1987, 38, 245–272; (d) Tong, Z.; Einaga, H.; Miyashita, H.; Fujita, H. Macromolecules 1987, 20, 1883–1887; (e) Bae, Y. C.; Soane, D. S.; Shim, J. J.; Prausnitz, J. M. J Appl Polym Sci 1993, 47, 1193–1206; (f) Cheluget, E. L.; Weber, M. E.; Vera, J. H. Chem Eng Sci 1993, 48(8), 1415–1426.
25. (a) Simha, R.; Somcynsky, T. Macromolecules 1969, 2, 342–350; (b) Nies, E.; Stroeks, A. Macromolecules 1990, 23, 4088–4092; (c) Zhong, C.; Wang, W.; Lu, H. Fluid Phase Equilib 1993, 83, 137–146.
26. (a) Shouten, J. A.; Ten Seldam, C. A.; Trappeniers, N. J. Physica 1974, 73, 556; (b) Kleintjens, L. A. Fluid Phase Equilib 1983, 10, 183; (c) Koningsveld, R.; Kleintjens, L.A.; Leblans-Vinck, A. M. J Phys Chem 1987, 91, 6423–6428.
27. (a) Sanchez, I. C.; Lacombe, R. H. J Phys Chem 1976, 80, 2352–2362; (b) Sanchez, I. C.; Lacombe, R. H. Macromolecules 1978, 11, 1145–1156; (c) Panayiotou, C.; Vera, J. H. Polymer J 1982, 14, 681–694; (d) Kumar, S. K.; Suter, U. W.; Reid, R. C. Ind Eng Chem Res 1987, 26, 2532; (e) High, M. S.; Danner, R. P.; Fluid Phase Equilib 1990, 55, 1–15; (f) Bawendi, M. G.; Freed, K. F. J Chem Phys 1988, 88, 2741–2756; (g) Freed, K. F.; Bawendi, M. G. J Phys Chem 1989, 93, 2194–2203; (h) Dickman, R.; Hall, C. J Chem Phys 1988, 85, 4108; (i) Hu, Y.; Lambert, S. M.; Soane, D. S.; Prausnitz, J. M. Macromolecules 1991, 24, 4356–4363; (j) Anderko, A. Int J Thermophys 1994, 15(6), 1221–1229; (k) Sanchez, I. C.; Balazs, A. C. Macromolecules 1989, 22, 2325–2331.
28. Dee, G. T.; Walsh, D. J. Macromolecules 1988, 21, 811.
29. (a) Beret, S.; Prausnitz, J. M. AIChE J 1975, 21, 1123–1132; (b) Morris, W.O.; Vimalchand, P.; Donohue, M. D. Fluid Phase Equilib 1987, 32, 103–115; (c) Kontogeorgis, G. M.; Harismiadis, V. I.; Fredenslund, Aa.; Tassios, D. P. Fluid Phase Equilib 1994, 96, 65–92.
30. (a) Chapman, W. G.; Gubbins, K. E.; Jackson, G.; Radosz, M. Fluid Phase Equilib 1989, 52, 31; (b) Huang, S. H.; Radosz, M. Ind Eng Chem Res 1990, 29, 2284–2294; (c) Chen, C.-K.; Duran, M. A.; Radosz, M. Ind Eng Chem Res 1993, 32, 3123–3127; (d) Wu, C. S.; Chen, Y. P. M .; Fluid Phase Equilib 1994, 100, 103–119.
31. (a) Hino, T.; Song, Y.; Prausnitz, J. M. Macromolecules 1994, 27, 5681–5690; (b) Song, Y.; Lambert, S. M.; Prausnitz, J. M. Macromolecules 1994, 27, 441–448; (c) Song, Y.; Hino, T.; Lambert, S. M.; Prausnitz, J. M. Fluid Phase Equilib 1996, 117, 69–76.
32. Chien, C. H.; Greenkorn, R. A.; Chao, K. C. AIChE J 1983, 29, 560.
33. (a) Prigogine, I.; Bellemans, A.; Mathot, V. The Molecular Theory of Solutions; North-Holland: Amsterdam, 1957; (b) Flory, P. J.; Orwoll, R. A.; Vrij, A. J Am Chem Soc 1964, 86, 3507–3514; (c) Patterson, D.; Delmas, G. Macromolecules 1969, 2(6), 672–677.

34. (a) Fredenslund, Aa.; Jones, R. L.; Prausnitz, J. M. AIChE J 1975, 24(1), 1086–1089; (b) Oishi, T.; Prausnitz, J. M. Ind Eng Chem Process Des Dev 1978, 17, 333–339; (c) Carvoli, G.; Castelli, A.; Marconi, A. M. Fluid Phase Equilib 1990, 56, 257–267; (d) Elbro, H. S.; Fredenslund, Aa.; Rasmussen, P. Macromolecules 1990, 23, 4707–4714; (e) Kontogeorgis, G. M.; Saraiva, A.; Fredenslund, Aa.; Tassios, D. P. Ind Eng Chem Res 1995, 34, 1823–1834; (f) Iwai, Y.; Shigematsu, Y.; Furuya, T.; Fukuda, H.; Arai, Y. Polym Eng Sci 1993, 33, 480–485.
35. (a) Heil, J. F.; Prausnitz, J. M. AIChE J 1966, 12(4), 678–685; (b) Brandani, V.; Macromolecules 1979, 12(5), 883–889; (c) Cui, Y.; Donohue, M. D. Macromolecules 1992, 25(24), 6489–6494; (d) Vetere, A. Fluid Phase Equilib 1994, 97, 43–52; (e) Lai, C. H.; Paul, D. R.; Barlow, J. W. Macromolecules 1988, 21, 2492–2502.
36. (a) Harismiadis, V. I.; Kontogeorgis, G. M.; Fredenslund, Aa.; Tassios, D. P. Fluid Phase Equilib 1994, 96, 93–117; (b) Saraiva, A.; Kontogeorgis, G. M.; Harismiadis, V. I.; Fredenslund, Aa.; Tassios, D. P. Fluid Phase Equilib 1995, 115, 73–93.
37. Vimalchand, P.; Donohue, M. D. J Phys Chem 1989, 93, 4355–4360.
38. Flory, P. J. Discuss Faraday Soc 1970, 49, 7–29.
39. Sandler, S. I. Models for Thermodynamics and Phase Equilibria Calculations; Marcel Dekker: New York, 1994; p 191.
40. Rebelo, L. P. N. Phys Chem Chem Phys 1999, 1, 4277–4286.
41. Bae, Y. C.; Soane, D. S.; Shim, J. J.; Prausnitz, J. M. J Appl Polym Sci 1993, 47, 1193–1206.
42. (a) Koningsveld, R.; Kleintjens, L. A. Macromolecules 1971, 4, 637–641; (b) Gundert, F.; Wolf, B. A. In Polymer Handbook; Brandrup, J.; Immergut, E. H., Eds.; Wiley: New York, 1989; (c) Eichinger, B. E. J Chem Phys 1970, 53, 561; (d) Kamide, K. Thermodynamics of Polymer Solutions. Phase Equilibria and Critical Phenomena; Elsevier: Amsterdam, 1990; (e) French, D. M. J Polym Sci Part C: Polym Lett 1988, 26, 469.
43. Orwoll, R. J. Rubber Chem Technol 1977, 452, 50.
44. (a) Koningsveld, R.; Staverman, A. J. J Polym Sci Part A.2 1968, 6, 305–325; (b) Riedl, B.; Prud'homme, R. E. J Polym Sci Polym Phys Ed 1988, 26, 1769; (c) Barton, A. F. M. Handbook of Polymer-Liquid Interaction Parameters and Solubility Parameters; CRC Press: Boca Raton, FL, 1990; (d) Brandrup, J.; Immergut, E. H. Polymer Handbook, 3rd ed.; Wiley: New York, 1989.
45. Cheluget, E. L.; Weber, M. E.; Vera, J. H. Chem Eng Sci 1993, 48(8), 1415–1426.
46. Gibbs, J. W. The Scientific Papers of J. Willard Gibbs; Dover Publications: New York, 1961; Vol. 1.
47. de Sousa, H. C.; Rebelo, L. P. N. Proceedings of the 3rd ISASF Congress; Brunner, G.; Perrut, M.; Eds.; Strasbourg, October 1994, Tome 1; pp 295–300.
48. (a) Chee, K. K. J Appl Polym Sci 1981, 25, 4299–4305; (b) Kiran, E.; Zhuang, W. J Supercrit Fluids 1994, 7, 1–8; (c) Hu, Y.; Ying, X.; Wu, D. T.; Prausnitz, J. M. Fluid Phase Equilib 1995, 104, 229–252.
49. Koningsveld, R.; Staverman, A. J. J Polym Sci Part A.2 1968, 6, 349–366.
50. (a) Gualtieri, J. A.; Kincaid, J. M.; Morrison, G. J Chem Phys 1982, 77, 521; (b) Salacuse, J. J.; Stell, G. J Chem Phys 1982, 77, 3714; (c) Briano, J. G.; Glandt, E. D. Fluid Phase Equilib 1983, 14, 91.
51. (a) Lustig, S. R.; Caruthers, J. M.; Peppas, N. A. Chem Eng Sci 1992, 47(12), 3037–3057; (b) Cotterman, R. L.; Bender, R.; Prausnitz, J. M. Ind Eng Chem Proc Des Dev 1985, 24, 194–203; (c) Willman, B. T.; Teja, A. S. AIChE J 1986, 32(12), 2067–2078; (d) Du, P. C.; Ali Mansoori, G. Fluid Phase Equilib 1986, 30, 57–64; (e) Ying, X.; Ye R.; Hu, Y.; Fluid Phase Equilib 1989, 53, 407–414; (f) Kramarz, J.; Wyczesany, A. Chem Eng Sci 1993, 48(9), 1665–1673.
52. (a) Szydlowski, J.; Van Hook, W. A. Macromolecules 1991, 24(17), 4883–4891; (b) Szydlowski, J.; Van Hook, W. A. J Polym Sci Part B: Polym. Phys 1991, 29, 1437–1439; (c) Szydlowski, J.; Rebelo, L. P.; Van Hook, W. A. Rev Sci Instrum 1992, 63(2), 1717–1725.
53. Guggenheim, E. A. Application of Statistical Mechanics; Clarendon Press: Oxford, U.K, 1966.
54. (a) Bigeleisen, J. J Chem Phys 1961, 34, 1485; (b) Jancsó, G.; Van Hook, W. A. Chem Rev 1974, 74, 689; (c) Jancsó, G.; Rebelo, L. P. N.; Van Hook, W. A.; Chem Rev 1993, 93, 2645–2666; (d) Jancsó, G.; Rebelo, L. P. N.; Van Hook, W. A. Chem Soc Rev 1994, 23, 257–264; (e) Bigeleisen, J.; Cragg, C. B.; Jeevanandam, M. J Chem Phys 1967, 47, 4335–4346.